Journal of Biophotonics

JOURNAL OF BIOPHOTONICS

RESEARCH ARTICLE OPEN ACCESS

Mid-IR Imaging Can Detect Waste Heat Production in the Nematode *Caenorhabditis elegans*

Ryan A. Merritt[1] | Kegan Heaney[2] | Nuren Shuchi[2] | Kacy L. Gordon[1] | Susan R. Trammell[2]

[1]Department of Biology, UNC Chapel Hill, Chapel Hill, North Carolina, USA | [2]Department of Physics and Optical Science, UNC Charlotte, Charlotte, North Carolina, USA

Correspondence: Kacy L. Gordon (kacy.gordon@unc.edu) | Susan R. Trammell (srtramme@charlotte.edu)

Received: 17 February 2025 | **Revised:** 22 April 2025 | **Accepted:** 24 April 2025

Funding: This work was supported by the National Institutes of Health.

Keywords: *C. elegans* | imaging of living organisms | label-free imaging | metabolism | mid-IR imaging | thermal imaging

ABSTRACT

Organisms carry out metabolic processes to produce chemical energy, but these biochemical pathways are inherently inefficient, resulting in the loss of energy as heat. This study reports the first characterization of the thermal signature of waste heat production in the ectothermic invertebrate *Caenorhabditis elegans* using thermal infrared (8–10 μm) imaging. A label-free imaging approach was developed to distinguish the heat output of living versus dead *C. elegans* by employing a cold object in reflectance mode with a highly reflective imaging substrate to suppress the thermal background. This method reveals a clear, repeatable difference in both the thermal output and cooling rate of living versus dead worms. Fourier Transform Infrared (FT-IR) spectroscopy confirms that the measured temperature differences arise from variations in kinetic temperature rather than differences in thermal emissivity. This novel approach provides a powerful tool for studying the previously inaccessible thermal biology of small ectothermic invertebrates.

1 | Introduction

Endothermic animals, such as mammals, regulate body temperature through metabolic processes to maintain homeostasis, whereas ectothermic organisms depend on environmental conditions to stay within a viable temperature range. For example, reptiles bask in sunlight to raise their body temperature and seek shade to cool down [1]. Most research on heat production, retention, and loss has focused on endothermic animals [2], while studies on ectotherm temperature regulation primarily examine heat exchange with the environment and its effects on metabolism.

Regardless of thermoregulatory strategy, metabolic pathways are inherently inefficient, with a portion of the total energy throughput lost as waste heat. When waste heat can be measured, it provides valuable insight into the metabolic state of the organism being studied. Previous studies have utilized thermal infrared (IR) imaging to investigate temperature regulation and metabolism in large endothermic animals [2]. In these animals, waste heat is a small contributor to body temperature relative to the production of heat by specialized molecular pathways that act to maintain body temperature. In contrast, detecting waste heat production in ectothermic animals, which lack such thermoregulatory pathways, could provide a more direct approach to studying their metabolic processes. However, there is a notable absence of literature on the thermal output of ectotherms, particularly invertebrates, likely due to the challenges in measuring the small amounts of heat generated by individual, small organisms. This study quantifies heat production in the small (1 mm), ectothermic invertebrate nematode worm, *Caenorhabditis elegans*.

C. elegans are longstanding genetic model organisms that share metabolic processes with human biomedical relevance [3, 4].

Many of the genes in the *C. elegans* genome have orthologs in humans, which makes it a useful model for studying conserved pathways [5–7]. Metabolism in *C. elegans* is currently measured using a set of complex techniques including the measurement of carbon dioxide production, oxygen consumption, and microcalorimetry [8–10]. These methods only provide resolution at the population level, and these three methods cannot be used simultaneously on the same population of organisms. Microcalorimetry requires an undisturbed assay medium, while measuring oxygen consumption requires consistent stirring, and the measurement of carbon dioxide production requires a sealed container [8–10]. Each of these methods attempts to relate the amount of an input to or output of metabolism mathematically to the overall metabolic rate of *C. elegans* and must make assumptions about metabolic efficiency.

In this study, a new, label-free thermal IR (8–10 μm) imaging technique to detect the waste heat produced by *C. elegans* is described. *C. elegans* are approximately the same temperature as their environment, and any thermal signal resulting from metabolic activity is likely small (<1°C). As a result, they are not easily distinguished from the thermal background when viewed in the infrared. Our imaging method suppresses thermal background without altering the worms' temperatures. To achieve this, a cold object was used in reflectance mode to mitigate thermal background interference. Worms were mounted on a silver-coated glass slide with low thermal emissivity, and radiation from the cold object was reflected off the slide. This made the slide appear cold, while the worms, being nonreflective, remained thermally distinct. We compared the difference in heat output between living and dead *C. elegans*. We hypothesize that dead worms should be cooler than living worms, as their major metabolic processes have stopped. We found that they are indeed cooler–and cool more slowly (as predicted by Newton's law of cooling). Fourier Transform Infrared (FT-IR) Spectroscopy was used to compare the reflectivity of live versus dead worms, ensuring that observed temperature differences were due to variations in kinetic temperature rather than differences in thermal reflectance or emissivity. Here, we demonstrate that very small ectothermic invertebrates generate detectable amounts of heat and that this heat can be accurately measured using our approach.

2 | Materials and Methods

2.1 | Worm Rearing

C. elegans of the N2 wild-type strain were picked at larval stages to generate an age-matched cohort for imaging at the young adult stage (2 days later at 20°C). Worm stages were determined via visual inspection under a dissecting microscope [11], and worms were transferred to *Escherichia coli* OP50-seeded NGM agar plates using a small wire implement [11]. Living *C. elegans* were directly compared to dead organisms from the same population in this study.

2.2 | Imaging System and Procedures

Because the *C. elegans* are nearly at the same temperature as their environment, suppressing thermal background is essential. However, the worms could not be placed directly onto a cold surface for imaging, as this would alter their metabolic processes or prove lethal. Instead, the worms were positioned on a highly reflective surface (a silver-coated glass slide; Kevley Technologies, Low-e Microscope Slides, L1272249. Fisher catalog number NC0733469) with a cold object (a metal pocket containing dry ice) mounted opposite to the camera (see Figure 1A). The silver-coated glass reflects the thermal radiation from the cold object into the camera, while the worms do not reflect this light. As a result, the thermal signature of the worms can be distinguished from the background.

Prior to imaging, a liquid drop of melted 2% w/v agarose/water was deposited onto the imaging substrate and compressed lightly with a borosilicate glass slide to make a thin agar pad. The agar pad was split in the middle using a micro pipette tip to form a humidified channel to prevent desiccation of the worms during imaging. *C. elegans* were then deposited directly onto the silver-coated slide in the middle of the channel (see Figure 1B). To obtain accurate and repeatable measurements, the region around the worms after they were placed in the channel had to be free of fluid and agar. The agar pad also proved to be a convenient control region to which we could compare the temperature of the worms to normalize across imaging runs.

A FLIR SC600 series mid-IR camera (sensitive from 7.5 to 12.0 μm) with an array size of 640 × 480 pixels and a maximum frame rate of approximately 200 fps was used to obtain images. The camera has a thermal resolution of approximately 20 mK, allowing detection of temperature differences at this scale within a single image. To utilize this sensitivity, 2–3 live worms were imaged alongside 2–3 dead controls on a single slide. Temperature differences between the worms from only this slide were then measured. This procedure was repeated for multiple slides. Absolute temperatures across the slides were not compared as this would require difficult/impossible absolute temperature calibration. The camera was rigidly mounted at an angle of 25° as measured from the vertical. This angle was measured at the start of each imaging session. A compound germanium lens system with an effective focal length of 100 mm was used with the camera, yielding a spatial resolution of 0.1 mm/pixel and a working distance of approximately 5 cm. The spatial resolution was confirmed by imaging a resolution standard. *C. elegans* adults are approximately 1–2 mm long and 0.2–0.5 mm wide, so our spatial resolution was sufficient to resolve the worms.

A cold object (anodized aluminum pocket filled with dry ice; $T \approx -78.5$°C) was mounted opposite the camera (at −25° as measured from the vertical). The imaging substrate reflected the thermal emission from this cold object into the camera, while less reflective objects, such as the *C. elegans* and agar, mounted on the imaging substrate failed to reflect as much of this thermal radiation. The use of the cold object in reflectance imaging mode suppressed background thermal emission. Without the cold object, the *C. elegans* could not be seen against the thermal background in the images [12].

Thermal imaging was executed during four different imaging sessions: December 2022, February 2023, July 2023, and December 2023 (Replicates 1, 2, 3, and 4, respectively). For

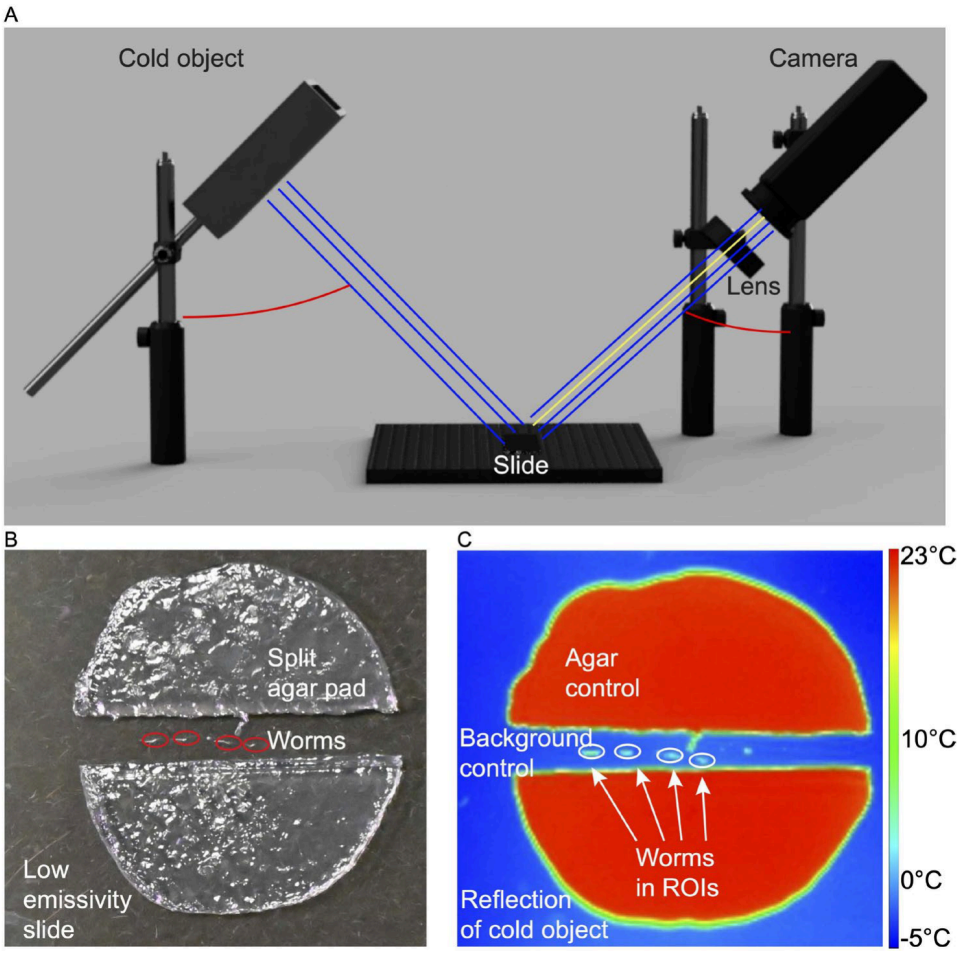

FIGURE 1 | A thermal imaging setup to record the heat output of *Caenorhabditis elegans*. (A) Schematic of imaging setup. A thermal camera is mounted at a 25° angle from vertical (red arc) above the imaging stage, with a cold object 25° from the vertical (red arc) on the opposite side of the sample allowing reflectance of the cold object (blue lines), isolating thermal signal from the worm (yellow line). (B) An agar pad was split to create a moist channel in which to mount the worms. (C) Background suppression allows the visualization of *C. elegans* worms in the thermal IR.

Replicates 1 and 2, two slides were prepared simultaneously by two researchers. One researcher picked up to four worms from a growth plate and placed them into the channel in the agar pad, and these animals were killed. The second researcher picked up to four worms from a growth plate and placed them into the channel in the agar pad on a different slide. These two slides were then imaged side-by-side. For Replicates 3 and 4, a single slide with two dead worms and two live worms was used. A researcher picked four worms into the agar channel on a single slide and then killed two of these worms. This single slide was then imaged. For all replicates, worms were killed by crushing their head with the wire pick used to move them. Crushing of the head resulted in no further movement of individual worms. Once movement and pharyngeal pumping had ceased, the worms were considered dead. Imaging began approximately 1 min later. Worms were only used if they remained intact after killing; those with a fully burst cuticle or extruded organs were removed from the imaging substrate. Ambient temperatures in the lab varied from 20°C to 24°C during all studies.

Imaging was acquired at frame rates of 6–24 Hz for this study. The camera was controlled by a Windows PC running FLIR ResearchIR software (Teledyne FLIR LLC) that interfaced with the camera via an ethernet connection. In all cases, 15–60 s videos were recorded and the temperatures of the worms, agar, and background as a function of time were determined from the individual frames of the video. By acquiring multiple frames per second, we could average across frames to minimize noise.

2.3 | Data Analysis

Temperature data was extracted from the individual frames of the video into a matrix. A MatLab (MathWorks Inc.) script was written to allow an ROI to be drawn around each worm. Within this ROI, a threshold was used to isolate pixels associated with the worm from pixels from the background. Three different thresholding criteria were used to extract temperature information for each *C. elegans*: all pixels above 80% of the maximum temperature, all pixels above 90% of the maximum temperature, and the maximum value within the ROI. ROIs were also placed on the agar pad and the slide background. A function was included in this script to allow the ROI to be reviewed throughout the video for the living worms to ensure they remained within the ROI (living worms can crawl away).

An average temperature of the worm was calculated over a 5-s period using all three thresholding techniques. The first 5 s of each video were used, as cooling due to the presence of the cold object used to quench the thermal background was minimal during this period. In addition to the 15-s videos captured for most imaging runs, several runs were imaged for 60 s. This allowed the cooling of both the worms and agar to be examined over a longer period of time. ROI temperatures were extracted for each frame of these longer videos.

2.4 | FT-IR Spectroscopy

FT-IR spectroscopy was used to characterize the reflectivity of both live and dead 2-day adult *C. elegans* as well as the agar pad. A HYPERION 3000 infrared microscope (Bruker Inc.), in combination with a VERTEX 70 Fourier-transform infrared spectrometer (Bruker Inc., Billerica, MA, USA), was used for all FT-IR measurements. A silicon carbide globar was the infrared light source. The 15× Cassegrain objective, with a square $20 \times 20\,\mu m$ aperture provided an average angle of incidence of 8.7° on the sample with an angular spread of 0.6°. Reflection measurements were taken in the infrared spectral range from 6 to 12 μm (833–1667 cm_{-1}), with resolution of 2 cm_{-1}. Acquisition of an FT-IR measurement took 60 s. Therefore, a chemical paralytic (sodium azide), was used to prevent motion of live worms during acquisition. The same paralytic was applied to dead worms so that it did not influence the resulting reflectivity measurement by altering the water content of the sample. Spectra of dead worms without the paralytic were also obtained and no differences in the spectra were noted for worms with or without the sodium azide. Emissivity spectra for multiple live and dead worms were acquired to account for minor variations in water content.

3 | Results

3.1 | Recorded Temperature Differences From Reference Substrate Show That Live Worms Are Warmer Than Dead Worms

We first calculated temperature differences between worms and the agar pad they were mounted beside. We then compared the background-subtracted temperatures of living worms to worms killed by a wire pick crushing the head (see Figures 1B and 2A). We subtracted the temperature of the worm from the agar pad to account for fluctuations in ambient temperature, and to capitalize on the high accuracy of the thermal camera for measuring temperature differences within a field (rather than absolute temperatures). Output of a linear mixed model (LMM) with replicate and slide as random effects and state (live/dead) as a fixed effect estimates dead worms differ in temperature from live worms by −0.95°C (95% CI −1.21 to −0.70; df = 308.68, $t = -7.42$, $p < 1 \times 10_{-12}$; Table 1). Individual LMM outputs for each replicate with slide as a random effect and state as a fixed effect are shown in Table 1 and graphed in Figure 2B. For all analyses, the 95% confidence interval lower and upper range have the same sign, suggesting that we can confidently refute the hypotheses that dead and live worms have the same temperature, or that dead worms are warmer than live worms. This trend of dead worms being cooler than their live counterparts was consistent across multiple thresholding methods. Thresholding methodology is described in the Methods section.

3.2 | Live Worms Cool Faster Than Dead Worms

Next, we sought an independent line of evidence that the starting temperatures of live and dead worms were different and that live worms were warmer. After worms are moved to the imaging platform, they are exposed to open air and sit near the cold pocket of dry ice, so they begin to cool. We used Newton's Law of cooling, which states that the larger the difference in an object's temperature compared to the surroundings, the faster the object will cool. Newton's law of cooling is given by Equation (1)

$$\frac{dT}{dt} = k\left(T - T_s\right) \tag{1}$$

where T is the temperature of the object of interest, T_s is the temperature of the surrounding environment, and k is a constant. To create cooling curves, we first normalized the temperature data from the 60-s videos to the starting temperature (average of the first five frames) in each video. This normalized data was then averaged across samples frame-by-frame for the living worms ($N = 32$) and similarly for the dead worms ($N = 32$; see Figure 2C). To quantify the rate of cooling, an exponential function (with form $T(t) = a^* e^{-\tau * t}$) was fit to each cooling curve. The cooling constant, τ, describes the rate of cooling, with larger τ indicating a faster rate of cooling. The cooling constants were $\tau = 0.0023\,s_{-1}$ for living worms and $\tau = 0.0018\,s_{-1}$ for dead *C. elegans* (as determined via a nonlinear regression; RMSE = 0.004 for both fits). The living worms cooled more quickly than the dead worms, meaning that the initial temperature of the living worms was higher than that of the dead worms.

In addition, the cooling of individual worms was also examined. An exponential curve was fit to the normalized temperature versus time curve for each individual worm. This analysis was performed using the 80% of maximum threshold, the 90% of maximum threshold, and the maximum temperature and an average value of τ was determined for living worms, $< \tau > = 0.0024 \pm 0.0002\,s_{-1}$, and dead worms, $< \tau > = 0.0019 \pm 0.0002\,s_{-1}$, for all thresholds. The p value for the two-tailed T-test (assuming equal variance) was ≤0.02 for all thresholding techniques, indicating that the observed difference in the cooling rates between living and dead worms is statistically significant. The details for the results of the t-tests are provided in Table 2.

3.3 | The Thermal Emissivities of Living and Dead Worms Do Not Differ

We wanted to control for a potential nonthermal difference between living and dead worms that could be driving the appearance of a temperature difference. The thermal camera measures the radiant temperature, T_R, of an object which is related to the kinetic temperature, T_K, by

$$T_R = \varepsilon^{\frac{1}{4}} T_K \tag{2}$$

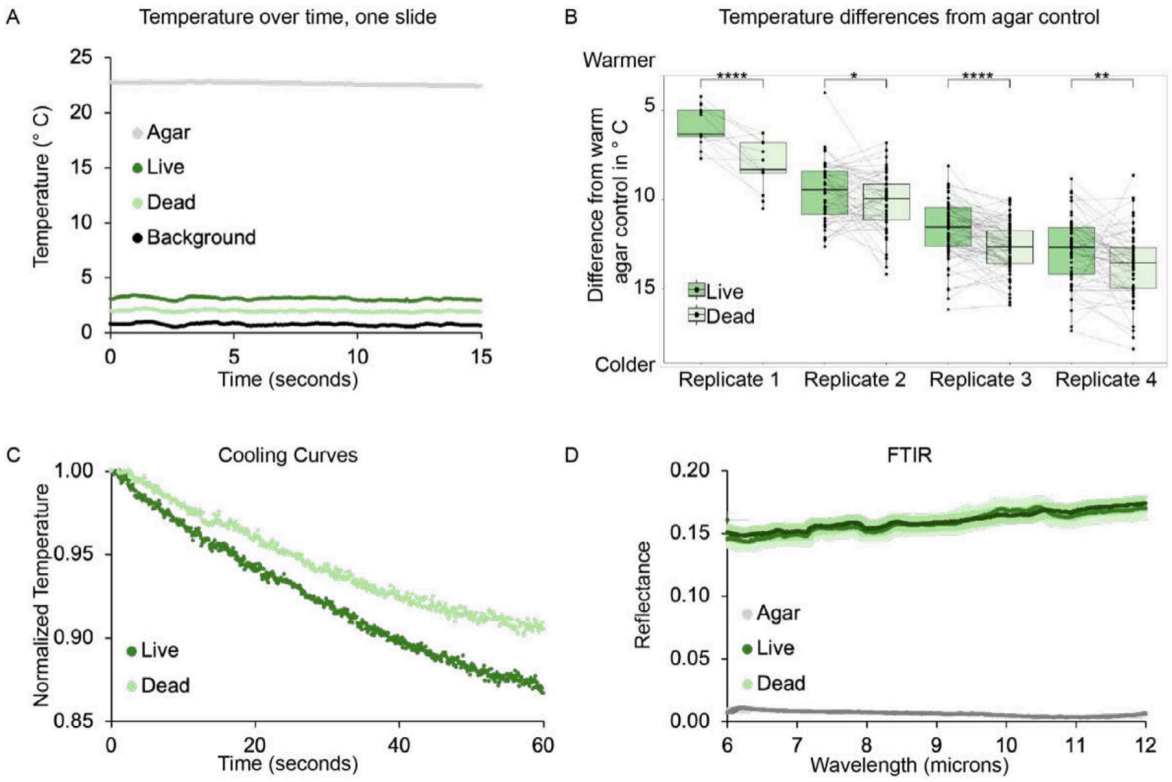

FIGURE 2 | Live worms are consistently warmer than dead worms, and this is not an artifact of different thermal emissivity. (A) Temperatures extracted from one representative 15 s acquisition, shown as a function of time for agar (gray), slide background (black), a representative live worm (dark green) and a representative dead worm (light green). (B) Boxplots showing all data from the 80% maximum temperature threshold for live (dark green) and dead (light green) worms for each of four replicates. Temperature is shown as temperature difference from the warmer agar (see A) control from the same slide. Smaller numbers are warmer temperatures. Boxes show mean and interquartile range and whiskers show 95% CI. Gray lines link measurements of worms imaged simultaneously on the same slide. Note the consistency in the direction of the slope; in 67/90 slides, the live worm was warmer than the dead worm. Significance asterisks come from individual LMMs (see Table 1) (C) Average cooling curves for living ($N = 32$) and dead ($N = 32$) worms using the 80% maximum temperature threshold showing the temperature of the worms (normalized to their temperature in Frame 1) as a function of time. Living worms cool more quickly than dead worms. The cooling constants were $\tau = 0.0023\,s^{-1}$ for living worms and $\tau = 0.0018\,s^{-1}$ for dead *Caenorhabditis elegans* (determined via nonlinear regression; RSME = 0.004 for both live and dead). (D) Average reflectance for living and dead *C. elegans* and the agar measured over the wavelength range of the thermal camera used to acquire other images for this study (live $N = 6$, dead $N = 7$, agar $N = 6$; shading indicates the 95% CI.) Curves fully overlap.

TABLE 1 | Linear mixed model analyses of replicates.

Replicate	ΔT live vs. dead[a]	95% CI lower	95% CI upper	df[b]	t value	$p_r(>\|t\|)$
1	−2.08	−2.77	−1.38	20.14	−5.87	9.43×10^{-6}
2	−0.61	−1.09	−0.13	87.11	−2.50	1.41×10^{-2}
3	−1.06	−1.43	−0.68	110	−5.51	2.41×10^{-7}
4	−0.88	−1.40	−0.35	88.29	−3.27	1.54×10^{-3}

[a]Temperature differences (ΔT) measured in °C.
[b]Satterthwaite approximation.

where ε is the emissivity of the object and temperatures are in K. Materials emit, reflect and transmit incident radiation, such that the sum of the emissivity, transmissivity, and reflectivity is 1. A higher reflectance would make an object appear artificially cooler due to its lower emissivity. FT-IR spectroscopy was used to measure reflectivity, from which emissivity can be estimated, to test whether living and dead worms differ in their optical properties in the thermal IR. In the case of *C. elegans* which have a large water content, the amount of transmitted IR light is low, so that the sum of the emissivity and reflectivity will be approximately 1. We measured the reflectance spectra of live ($N = 6$) and dead ($N = 7$) worms over the wavelength range of the thermal camera 7.5–12 μm (Figure 2D). The average reflectance of living *C. elegans* was 16.3% (95% CI: 15.7%–16.9%) and that of dead *C. elegans* was 16.2% (95% CI: 15.6%–16.8%). The measured temperature difference between living and dead *C. elegans* cannot be explained by differences in emissivity and is most likely the result of a true difference in kinetic temperature.

TABLE 2 | *T*-test results for comparison of cooling coefficients, τ, for live versus dead worms.

	80% threshold	90% threshold	Max threshold
df	66	66	66
T-stat	2.34	2.31	2.46
T-crit (two tail)	1.99	1.99	1.99
p (two tail)	0.022	0.024	0.017

Notice that in Figure 2A, the measured radiant temperature of the agar is warmer than the radiant temperatures of both living and dead *C. elegans*. This was true for all images. The kinetic temperature of the dead worms and agar should be the same (both had equilibrated to room temperature before images were taken, and we predict that dead worms cease to produce heat). The measured difference in radiant temperature is therefore due to a difference in the emissivity of the worms versus the agar (see Equation 2). FT-IR spectra ($N=6$) of the agar were acquired and the average reflectance of the agar pad over the 7.5–12 μm range was 0.24% (95% CI: 0.24207%–0.24210%). Calculating radiant temperatures with the measured emissivities of the agar versus worms, we find that the greater reflectivity of the worms will cause their radiant temperatures to appear over 12 K degrees cooler than the agar at room temperature (296 K). This predicted difference agrees with the difference in the measured radiant temperatures of dead worms and agar (see Equation (2) and Figure 2B in which the average difference in radiant temperature between dead worms and agar is just over 11°), bolstering our confidence that we can measure the temperatures of the worms accurately. It is worth noting that the minor difference in emissivities of live and dead worms as calculated by FTIR would bias our measurements of radiant temperature to make the dead worms appear slightly warmer than live worms, further building our confidence that our method is capturing real temperature differences between living and dead worms.

4 | Discussion and Conclusions

Our label-free thermal IR imaging technique detects that live worms are measurably warmer than dead worms, cool faster, and that this difference cannot be explained by differences in their thermal emissivity. There was a statistically significant difference in the temperatures of dead versus live worms, with the dead worms being cooler. Cooling curves demonstrated that the rate of cooling for living worms was faster than that of dead worms. According to Newton's law of cooling, this is evidence that the living worms had a higher initial temperature than the dead worms. FT-IR spectroscopy indicated that the thermal emissivity of living and dead *C. elegans* is the same, suggesting that the measured temperature difference between these two populations is a result of a true difference in kinetic temperature rather than an artifact of a difference in optical or thermal properties.

Previous studies of *C. elegans* using infrared techniques have focused on biochemical characterization. For example, FT-IR microspectroscopy has been employed to analyze scattering and absorbance properties related to the worms' biochemical composition [13, 14]. More recently, hyperspectral imaging in the mid-IR, enabled by quantum cascade lasers, has been used for similar purposes [15]. Near-IR infrared imaging has been used to study insect development in a chrysalis [16] and mid-IR imaging has been used to study the thermoregulatory function of butterfly wings [17]. However, to our knowledge, no prior studies have used passive thermal infrared imaging to directly measure endogenous heat production in *C. elegans* or other comparably sized invertebrates.

Indeed, the notion of endogenous heat production in an ectothermic animal as small as a nematode worm has not, to our knowledge, been considered in the literature. Current methods for measuring metabolism in *C. elegans*—including carbon dioxide production, oxygen consumption, and microcalorimetry—are limited to population-level resolution and cannot be applied simultaneously due to conflicting technical requirements. Each technique also relies on assumptions about metabolic efficiency to infer overall metabolic rate [8–10]. The thermal imaging technique described here yields insights that were inaccessible to these methods and eliminates assumptions made about metabolic efficiency required by these techniques. Thermal imaging also provides single-animal resolution, while current techniques are limited to the study of populations of animals, not individuals. Shortcomings of our new technique are its relatively low throughput and the challenges in measuring the small thermal signal. In the future, this technique could be used to compare *C. elegans* of different metabolic conditions (age, genotype, food source, exercised, drugged).

Author Contributions

R.A.M., K.L.G., and S.R.T. designed research. R.A.M., K.H., N.S., K.L.G., and S.R.T. performed research. R.A.M. and K.H. analyzed data. R.A.M. wrote the initial draft. K.L.G. and S.R.T. reviewed and edited the original manuscript.

Acknowledgments

Research reported in this publication was supported by the NIGMS of the National Institutes of Health under award number R35GM147704 to K.L.G. The authors would like to thank Cobey McGinnis, Anteneh Tsegaye, Gunnar Olson, and Madeline Kern (UNC Charlotte) for their assistance with constructing the imaging setup and with preliminary data analysis, and Dr. Tino Hofmann (UNC Charlotte) for his assistance with the FT-IR spectroscopy.

Conflicts of Interest

The authors declare no conflicts of interest.

Data Availability Statement

The data that support the findings of this study are available from the corresponding author upon reasonable request.

References

1. F. Seebacher and C. E. Franklin, "Physiological Mechanisms of Thermoregulation in Reptiles: A Review," *Journal of Comparative Physiology B* 175, no. 8 (2005): 533–541, https://doi.org/10.1007/s00360-005-0007-1.

2. D. J. McCafferty, C. Gilbert, W. Paterson, et al., "Estimating Metabolic Heat Loss in Birds and Mammals by Combining Infrared Thermography With Biophysical Modelling," *Comparative Biochemistry and Physiology Part A: Molecular & Integrative Physiology* 158, no. 3 (2011): 337–345, https://doi.org/10.1016/j.cbpa.2010.09.012.

3. B. C. Mullaney and K. Ashrafi, "*C. Elegans* Fat Storage and Metabolic Regulation," *Biochimica et Biophysica Acta (BBA)-Molecular and Cell Biology of Lipids* 1791, no. 6 (2009): 474–478, https://doi.org/10.1016/j.bbalip.2008.12.013.

4. K. T. Jones and K. Ashrafi, "Caenorhabditis Elegans as an Emerging Model for Studying the Basic Biology of Obesity," *Disease Models & Mechanisms* 2, no. 5–6 (2009): 224–229.

5. M. Uno and E. Nishida, "Lifespan-Regulating Genes in *C. Elegans*," *npj Aging and Mechanisms of Disease* 2, no. 1 (2016): 1–8.

6. H. G. Son, O. Altintas, E. J. E. Kim, S. Kwon, and S.-J. V. Lee, "Age-Dependent Changes and Biomarkers of Aging in *Caenorhabditis Elegans*," *Aging Cell* 18, no. 2 (2019): e12853.

7. S. Zhang, F. Li, T. Zhou, G. Wang, and Z. Li, "*Caenorhabditis Elegans* as a Useful Model for Studying Aging Mutations," *Frontiers in Endocrinology* 11 (2020): 554994.

8. B. P. Braeckman, K. Houthoofd, and J. R. Vanfleteren, "Assessing Metabolic Activity in Aging *Caenorhabditis Elegans*: Concepts and Controversies," *Aging Cell* 1, no. 2 (2002): 82–88, https://doi.org/10.1046/j.1474-9728.2002.00021.x.

9. W. A. Van Voorhies, "The Influence of Metabolic Rate on Longevity in the Nematode *Caenorhabditis Elegans*," *Aging Cell* 1, no. 2 (2002): 91–101.

10. R. Laranjeiro, G. Harinath, D. Burke, B. P. Braeckman, and M. Driscoll, "Single Swim Sessions in *C. Elegans* Induce Key Features of Mammalian Exercise," *BMC Biology* 15 (2017): 30.

11. A. K. Corsi, B. Wightman, and M. Chalfie, "A Transparent Window Into Biology: A Primer on *Caenorhabditis Elegans*," *Genetics* 200, no. 2 (2015): 387–407, https://doi.org/10.1534/genetics.115.176099.

12. R. A. Merritt, C. L. McGinnis, K. L. Gordon, and S. R. Trammell, "Label-Free Biomedical Imaging and Sensing (LBIS) 2023," 2023, SPIE 16–23.

13. W. Petrich, "Mid-Infrared and Raman Spectroscopy for Medical Diagnostics," *Applied Spectroscopy Reviews* 36, no. 2–3 (2001): 181–237.

14. A. Bouyanfif, S. Liyanage, E. Hequet, N. Moustaid-Moussa, and N. Abidi, "Review of FTIR Microspectroscopy Applications to Investigate Biochemical Changes in *C. Elegans*," *Vibrational Spectroscopy* 96 (2018): 74–82.

15. K. Haase, N. Kröger-Lui, A. Pucci, A. Schönhals, and W. Petrich, "Real-Time Mid-Infrared Imaging of Living Microorganisms," *Journal of Biophotonics* 9, no. 1–2 (2016): 61–66.

16. Z. R. Moran and A. G. Parker, "Near Infrared Imaging as a Method of Studying Tsetse Fly (Diptera: Glossinidae) Pupal Development," *Journal of Insect Science* 16, no. 1 (2016): 72.

17. C. C. Tsai, R. A. Childers, N. Shi Norman, et al., "Physical and Behavioral Adaptations to Prevent Overheating of the Living Wings of Butterflies," *Nature Communications* 11, no. 1 (2020): 551.